PAPER

Check for updates

Development and evaluation of 3D composite scaffolds with piezoelectricity and biofactor synergy for enhanced articular cartilage regeneration†

Bowen Xie, (ID) ‡[ab] Hebin Ma, (ID) ‡[cd] Fengyuan Yang, (ID) ‡[e] Hongguang Chen, (ID) ‡[d]
Ya'nan Guo,[d] Hongxing Zhang,[a] Tengfei Li,[a] Xiaogang Huang,[a] Yantao Zhao,*[d]
Xiaojie Li*[a] and Junjie Du*[abe]

The inability of articular cartilage to self-repair following injuries frequently precipitates osteoarthritis, profoundly affecting patients' quality of life. Given the limitations inherent in current clinical interventions, an urgent need exists for more effective cartilage regeneration methodologies. Previous studies have underscored the potential of electrical stimulation in cartilage repair, thus motivating the investigation of innovative strategies. The present study introduces a three-dimensional scaffold fabricated through a composite technique that leverages the synergy between piezoelectricity and biofactors to enhance cartilage repair. This scaffold is composed of polylactic acid (PLLA) and barium titanate (BT) for piezoelectric stimulation and at the bottom with a collagen-coated layer infused with fibroblast growth factor-18 (FGF-18) for biofactor delivery. Designed to emulate the properties of natural cartilage, the scaffold enables controlled generation of piezoelectric charges and the sustained release of biofactors. *In vitro* tests confirm that the scaffold promotes chondrocyte proliferation, matrix hyperplasia, cellular migration, and the expression of genes associated with cartilage formation. Moreover, *in vivo* studies on rabbits have illustrated its efficacy in catalyzing the *in situ* regeneration of articular cartilage defects and remodeling the extracellular matrix. This innovative approach offers significant potential for enhancing cartilage repair and holds profound implications for regenerative medicine.

1 Introduction

Articular cartilage is essential for smooth joint motion and protecting bones within synovial joints.[1] Due to its lack of blood vessels, nerves, and lymphatic tissues, the repair of cartilage presents significant challenges.[2,3] If not addressed promptly and effectively, cartilage damage may progress to osteoarthritis (OA), a degenerative disease. Current treatment modalities, including medication and surgical interventions,

primarily aim to mitigate symptoms yet fail to cure the underlying conditions.[4] This limitation highlights the imperative for pioneering strategies, such as cartilage tissue engineering.[5] This innovative approach employs a combination of seed cells, suitable materials, and physical cues embedded within scaffolds that emulate the natural extracellular matrix (ECM). These scaffolds provide not only a structural framework but also metabolic sites essential for tissue regeneration.[6–8]

Decades of research studies have underscored the stimulatory effects of piezoelectricity on cartilage.[9] It has been observed that cartilage generates bioelectrical signals during joint movement or when subjected to stress.[10,11] In response to these signals, an increase in chondrocyte proliferation and matrix production occurs, thereby facilitating cartilage repair. This indicates that electrical stimulation might replicate this natural environment to enhance repair processes.[12–14] Research has shown that electrical fields can promote proteoglycan synthesis, which strengthens the cartilage further.[15,16] However, traditional methods of delivering electrical fields are fraught with limitations, which has led to the development of innovative implantable

*a Department of Orthopedics, Air Force Medical Center, Beijing 100142, China.
E-mail: albertlxj@126.com*
*b Air Force Clinical College, The Fifth School of Clinical Medicine, Anhui Medical
University, Hefei 230032, China. E-mail: dujunjie205@hotmail.com*
c Medical School of the PLA General Hospital, Beijing 100853, China
*d Senior Department of Orthopedics, The Fourth Medical Center of the PLA General
Hospital, Beijing 100048, China. E-mail: biodoctor1981@163.com*
e Graduate School of Medicine, China Medical University, Shenyang 110122, China
† Electronic supplementary information (ESI) available. See DOI: https://doi.org/
10.1039/d4tb01319k
‡ These authors contributed equally to this work.

biological scaffolds possessing intrinsic electrical activity.[14,17,18] Piezoelectric materials, which respond to mechanical stress autonomously, are deemed ideal for this purpose in tissue engineering.

Commonly utilized piezoelectric materials comprise barium titanate (BT), sodium potassium niobate (KNN), zinc oxide (ZnO), polyvinylidene fluoride (PVDF), and poly L-lactic acid (PLLA). Among these, BT is distinguished due to its superior piezoelectric performance and biocompatibility.[19] Though not readily absorbable, it is capable of being retained in the body harmlessly for prolonged periods.[20] Furthermore, poly L-lactic acid (PLLA) is recognized for its mechanical properties and biodegradability.[21] To enhance cartilage regeneration under joint loading, researchers have developed PLLA-collagen scaffolds, thereby introducing a novel therapeutic approach.

Biofactors, such as fibroblast growth factor-18 (FGF-18), play a critical role in the regeneration of cartilage. Being predominantly found in organs including the lungs and kidneys, FGF-18 is essential for promoting the proliferation, differentiation, and maturation of chondrocytes, all of which are vital for maintaining the integrity of cartilage.[22–25] In preclinical models, FGF-18 has demonstrated the potential to enhance cartilage repair, particularly in cases of osteoarthritis. This is achieved through the stimulation of key ECM component production and the alleviation of symptoms.[26] Consequently, the application of FGF-18 could be significant in cartilage repair promoted by piezoelectricity.

Prior research has primarily focused on either the piezoelectric stimulation for cartilage regeneration[11,27–30] or the release of active factors to facilitate cartilage repair.[31–34] However, there has been no integration of piezoelectricity with biofactors that would synergize the electrical properties of PLLA and BT with the biological effects of FGF-18. The development of PLLA–BT composite nanofiber membranes through electrostatic spinning, which are designed to produce a high electrical output and simultaneously release FGF-18, presents a novel therapeutic strategy to enhance cartilage regeneration (Scheme 1).

2 Materials and methods

2.1 Materials preparation

2.1.1 Fabrication of nanofiber scaffolds by electrospinning. PLLA particles, sourced from Shenzhen Boli Biomaterials, China, were dissolved at a concentration of 10% (W/V) in hexafluoroisopropanol, provided by Shanghai Aladdin Biochemical Technology, China. Subsequently, barium titanate powder, from Nanostructured & Amorphous Materials, Inc., USA, possessing an average diameter of 400 nm, was introduced into the solution under ultrasound stimulation for one hour and stirred for an additional four hours, ensuring an adequate dispersion of BT within the mixture. This process resulted in the formation of a stable electrostatic spinning solution, containing 5% BT by weight of PLLA, as shown in Fig. S1–S3 (ESI†). The solution was then transferred to a syringe, positioned in an electrospinning machine, and extruded at a rate of 0.3 mm min^{-1}. The distance between the needle and the collector was maintained at 10.0 cm. During electrospinning, the syringe needle was energized to 16 kV and the collector end to −1 kV.[35] To fabricate aligned PLLA/BT films, the collector's rotation speed was set at 5000 rpm. The resultant aligned PLLA/BT nanofiber membrane was utilized as the outer layer of the piezoelectric scaffold. Discs with a diameter of 10 mm were prepared using a hole punch.
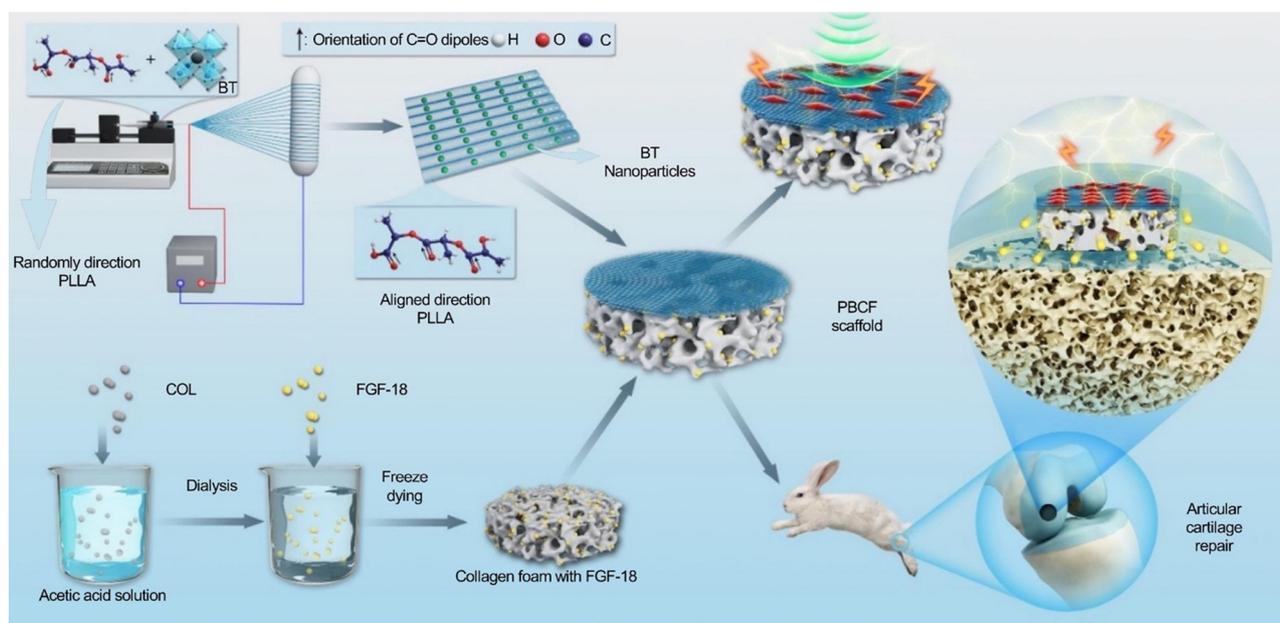
Scheme 1 A schematic diagram illustrating the manufacturing process and biological application of a three-dimensional composite scaffold that incorporates piezoelectric stimulation and synergistic bioactive factors.

This journal is © The Royal Society of Chemistry 2024

J. Mater. Chem. B, 2024, **12**, 10416–10433 | **10417**

2.1.2 Preparation of collagen membrane scaffolds encapsulating FGF-18. Microfibrillar bovine tendon type I collagen, supplied by Beijing Qingyuan Weiye Biological Tissue Engineering Co., was dissolved in 0.5 M anhydrous acetic acid (pH 2.8). The mixture was stirred until a 2% (W/V) collagen membrane was formed and the consistency became gelatinous. Subsequently, the pH was adjusted to 7.0 using NaOH solution for acid–base neutralization. The mixture was then centrifuged at high speed to remove excess materials. Following centrifugation, it underwent dialysis with deionized water being replaced every 6 hours for three days. After dialysis, 100 ng mL^{-1} of recombinant human FGF-18 factor was added and thoroughly mixed in the solution, which was then lyophilized at -80 °C to create a collagen/FGF-18 composite membrane. A 10 mm diameter foam membrane was also prepared using a perforator. Cross-linking was subsequently performed with EDC and NHS (Aladdin, China) for two hours at room temperature.[36] Multiple rinsing of the scaffolds was performed to remove water-soluble urea, a by-product of the reaction, thereby enhancing the stiffness of the collagen layer to adequately support the upper electrostatically spun film over time.

A layer of pure collagen solution was applied to the surface of the collagen/FGF-18 composite membrane. It was then laminated with the PLLA/BT piezoelectric nanofiber membrane to form a PLLA/BT/collagen/FGF-18 (PBCF) composite membrane. The composite was finally lyophilized at -80 °C.

2.2 Materials characterization

2.2.1 Physical characterization of PBCF composite scaffolds. Samples measuring 5×5 cm ($n = 5$) were prepared to observe the fiber morphology and microstructure within the composite scaffolds. These observations were conducted using a scanning electron microscope (SEM; E-1045, Hitachi, Japan) following gold sputter coating. The orientation of the fibers on the surface of the membranes was analyzed with the ImageJ software, measuring the orientation angles of all nanofibers relative to a predefined vertical direction ($0°$).[37] Additionally, the distribution of BT nanoparticles (NPs) within the PLLA fiber matrix was examined using transmission electron microscopy (TEM; FEI Talos F200X G2, US), and the chemical composition of the composite fibers was assessed using energy dispersive X-ray spectroscopy (EDS; EMAX EX-300 system).[38] Following a drying period of 24 hours at 40 °C, the PBCF composite scaffolds were further characterized using Fourier transform infrared spectroscopy (FTIR; Ettlingen, Germany). Crystal structures of the samples were investigated using X-ray diffraction (XRD; Rigaku Smartlab, Japan), with a scan rate of $2°$ min^{-1} and a data collection ranging from $5°$ to $70°$.[35]

The mechanical properties of the PBCF composite supports were evaluated using a uniaxial tensile tester (Shandong Wanchen Testing Machine Co., Ltd, China). Samples, each measuring 5.0×1.0 cm^2 with an approximate thickness of 0.3 mm ($n = 3$), were subjected to a stretching rate of 5 mm per minute until fracture.[35] The Young's modulus and tensile strength were derived precisely from the stress–strain curves. Mechanical properties were recorded for at least three specimens and the results were averaged.

2.2.2 Measurement of piezoelectric properties. The piezoelectric output of the aligned PLLA/BT films was quantified using a high-impedance electrostatometer (Keithley 6517B, Cleveland, OH, USA) under an impact force of 30.0 N. These piezoresponsive materials were subjected to characterization and morphological analysis at the nanoscale using piezoresponse force microscopy (PFM; Bruker Dimension ICON, Beijing). Initially, a PLLA/BT nanofiber membrane was secured onto a mica sheet on the stage of the microscope. Piezoelectric properties were then demonstrated through PFM switching, involving the application of a DC-biased triangular sweep modulated by square wave signals to alter local polarization. Subsequently, the intensity and spatial distribution of the piezoelectric signals were meticulously recorded.

2.2.3 Assessment of loading and release of FGF-18. To evaluate the release of FGF-18, PBCF samples were immersed in 1 mL of phosphate-buffered saline (PBS) at a pH of 7.4.[39] One group was maintained under static conditions without intervention, while the other group received ultrasonic (US) stimulation for 10 minutes each during morning and afternoon sessions (consistent with the protocols of associated animal studies, the US stimulation was applied only on weekdays). Both groups were incubated at 37 °C. At predetermined intervals (1, 3, 7, 14, 21, and 28 days), 50 μL of the supernatant was collected and immediately stored at -80 °C, after supplementation with an equivalent volume of PBS. The FGF-18 concentration in the PBS was quantified at each time point using a human FGF-18 ELISA kit (Yang Guang Ying Rui, Beijing), adhering strictly to the manufacturer's instructions. The detection threshold was established at 20 pg mL^{-1}. Protein recovery rates were normalized against a control sample of FGF-18, deemed to represent 100% recovery, based on the ELISA data.

2.3 *In vitro* studies of PBCF composite scaffolds

2.3.1 Isolation and culture of articular chondrocytes. Ethical approval for all animal experiments was obtained from the Ethics Committee of Keyu Animal Breeding Center, Beijing, China (Approval No. KY20230613003). Chondrocytes were harvested from the knee joints of 1–2 week-old New Zealand white rabbits using established protocols.[8] These cells were then cultured in the DMEM/F-12 medium, which was enriched with 1.0% penicillin/streptomycin (Bost Biotech Co., Ltd, Wuhan, China) and PBCF composite scaffolds. The culture medium was replenished every three days.

Localized electrical signals were induced by subjecting the culture plates to ultrasonic homogenization, with the ultrasonic parameters set to 200 W for 20 minutes daily, divided into two sessions of 10 minutes each in the morning and afternoon. This 200 W setting was chosen based on prior investigations that demonstrated a stable piezoelectric output and enhanced proliferation of chondrocytes at this intensity level.

Further details on chondrocyte extraction methods and experimental setups are provided in our previous study.[37]

10418 | *J. Mater. Chem. B*, 2024, **12**, 10416–10433

This journal is © The Royal Society of Chemistry 2024

2.3.2 Chondrocyte seeding on scaffolds and US stimulation. PBC-based scaffolds, PBCF scaffolds, and their respective US stimulation groups were designated as subgroups for the entirety of the experiment. Articular chondrocytes were cultured in the normal medium and inoculated at a density of 1×10^4 cells per well. These cells were evenly distributed across 48-well plates, with four replicate wells for each group. To each well, 500 μL of the DMEM/F-12 (Wuhan Bioengineering Medium, China) supplemented with FBS (Shanghai Biotechnology, China) was added. Ultrasound stimulation was administered for a duration of 20 minutes daily over a period of 14 days at a power setting of 200 W. The duration of the intervention was consistently maintained at 20 minutes for both *in vitro* US stimulation and *in vivo* motile cartilage repair experiments. On days 3, 5, and 7, 50 μL of the cell counting kit-8 (CCK-8) (Abmole, USA) reagent was added to each well, followed by an incubation period of 2 hours and subsequent absorbance (ABS) measurements.

Live/dead assays were executed in accordance with established protocols on 48-well plates. Each set of piezoelectric composite scaffolds was cultured with chondrocytes at a concentration of 1×10^4 cells mL^{-1} and maintained at 37 °C in an atmosphere of 5.0% CO_2 humidity until day 3. The cells were subjected to ultrasonic vibrations for 20 minutes daily. Afterward, the samples were washed three times with PBS and double-stained with calcein acetoxy methylester/propidium iodide for 30 minutes at room temperature, protected from light exposure. The adhesion and cellular activity of the articular chondrocytes on the various materials were subsequently observed using a fluorescence microscope.

2.3.3 Morphology of chondrocytes on the scaffold cytotoxicity test. The chondrocytes were cultured for three days, during which their adhesion to the nanofiber surface was evaluated using actin staining. Following the culture period, the material was rinsed with a PBS solution and then fixed with 4% paraformaldehyde for 20 minutes. Subsequently, it was washed three times with PBS. The nanofiber scaffold underwent treatment with 0.1% Triton X-100 for 20 minutes and was washed three times with PBS thereafter.[37] Staining of the scaffold–cell complex was performed according to the instructions provided with the staining kit. Cytoskeletal protein (F-actin) was stained using phalloidin, and nuclei were labeled using a 4′,6-diamidino-2-phenylindole (DAPI) staining solution. Observations of the staining were conducted using a fluorescence microscope.

2.3.4 Chondrocyte ECM secretion capacity assay. Following the inoculation of chondrocytes into each scaffold group, they were cultured *in vitro* for 3, 7, and 14 days. Subsequently, the samples were digested with a pre-prepared papain solution [125 mg mL^{-1} papain, 100 mM Na_2HPO_4, 5 mM ethylene diamine tetra-acetic acid (EDTA), pH 6.4] at 60 °C for 16 h.[37] Quantitative analytical detection of DNA, glycosaminoglycans, and hydroxyproline was then performed. The DNA content was measured using a Qubit Flex™ fluorometer (Thermo Fisher Scientific, United States), following the instructions of the DNA quantification kit. Given that the amount of hydroxyproline in collagen is fixed, the collagen content was inferred by evaluating the hydroxyproline content. Levels of glycosaminoglycans and

hydroxyproline in various scaffold groups were determined using ELISA kits (Jiubang Biotechnology, China). Finally, the ability of each group to secrete glycosaminoglycans and hydroxyproline per unit of DNA was calculated at each time point based on the DNA content.

2.3.5 Gene expression analysis. The procedures for RNA isolation and complementary DNA (cDNA) synthesis were conducted according to the kit instructions. RNA was isolated from chondrocytes using Trizol (Tiangen Biotech, China), and the total RNA was subsequently reverse-transcribed into cDNA. The quantification of cDNA was performed using a real-time quantitative PCR detector (Applied Biosystems QuantStudio™ 7 Flex, USA). Detailed protocols for these procedures are described in the study by Xie *et al.*[37] Glyceraldehyde 3-phosphate dehydrogenase was used as the internal reference gene for analyzing the gene expression of collagen type II (*COL-II*), aggregated protein (*ACAN*), and sex-determining region Y box protein-9 (*SOX-9*). The RT-qPCR primers used in this study are listed in Table S1 of the ESI.†

2.4 *In vivo* studies of PBCF composite scaffolds

2.4.1 Surgical procedures for rabbit's cartilage defect creation and scaffold implantation. As described in the literature,[11] 36 New Zealand white rabbits, each weighing between 2.5 and 3 kg, were randomly assigned to three groups: blank, PBC, and PBCF. Before the main experiment, a preliminary study involving two rabbits was performed to establish the postoperative protocol. Anesthesia was induced with 3% sodium pentobarbital, administered intravenously along the ear margins. After shaving and disinfection, both knee joints were surgically exposed *via* a medial incision to facilitate access to the joint, and soft tissues were retracted. The patella was displaced laterally to reveal the femoral condyles, and a grinding drill was used to create a cartilaginous defect, 4 mm in diameter and 3 mm deep, on the weight-bearing portion of the medial condyle of the knee joint. This location was chosen to ensure that the implanted scaffold could withstand the forces exerted during rabbit locomotion. Scaffolds of PBC and PBCF, precisely fitting the defect, were implanted. Following implantation, the joint was cleansed, and the muscle and skin were sutured closed. The wound was then covered with sterile gauze, and gentamicin sulfate was administered daily for three days. The rabbits underwent a recovery period of two weeks, after which they were conditioned to exercise on a treadmill at a speed of 1 kilometer per hour for 20 minutes daily, divided into two sessions (morning and afternoon), as shown in Video S1 (ESI†). Cartilage extraction was conducted at 4- and 8-weeks post-implantation. Ultimately, all rabbits were euthanized, and their knee joints were harvested for further analysis.

2.4.2 MRI analysis. Cartilage sampling was conducted at predetermined postoperative intervals of 4 and 8 weeks. Subsequently, all New Zealand rabbits were euthanized, and their knee joints were collected for analysis. The collected samples were then subjected to MRI scanning using a Bruker BioSpec 70/30 system (Germany). Following the imaging process, the evaluation of cartilage repair was performed utilizing

This journal is © The Royal Society of Chemistry 2024

J. Mater. Chem. B, 2024, **12**, 10416–10433 | **10419**

the Henderson MRI assessment method. This systematic approach ensured the objective assessment of the reparative outcomes in the cartilage.

2.4.3 Histological analysis. Following the conclusion of the MRI scan, the muscles and soft tissues surrounding the femoral condyles were meticulously excised, and digital images of the cartilage defect model were obtained. Histological analyses were conducted on three randomly selected specimens from each group at both 4- and 8- weeks post-procedure. These specimens were subjected to overnight immersion in 10% formalin, followed by decalcification, paraffin embedding, and cross-sectional staining at the center of the restoration sites. Morphological assessments and evaluations of inflammatory infiltrate were performed using hematoxylin and eosin (H&E) staining. Additionally, safranin O-fast green staining was utilized to examine the articular cartilage and sulfated glycosaminoglycans (GAGs).[40] To further investigate the characteristics of type II collagen, immunohistochemistry and immunofluorescence staining techniques were applied, using a monoclonal anti-collagen II antibody (Cell Signaling Technology, Boston, USA). Quantification of the regenerative tissue fill area and the glycosaminoglycan area was carried out using ImageJ (National Institutes of Health, Bethesda, MD, USA), in conjunction with the threshold tool.[41]

2.4.4 Score system to evaluate the degree of cartilage regeneration. The morphological evaluation of cartilage regeneration was independently conducted by three experienced professionals, who were proficient in cartilage histology and blinded to the experimental conditions. This evaluation was based on the International Cartilage Repair Society (ICRS) macroscopic evaluation of cartilage and the ICRS visual histological assessment scale.[42–44] Scores from all professionals were compiled for analysis.

2.5 Statistical analysis

A one-way analysis of variance (ANOVA) was utilized to compare multiple groups, with the LSD test serving as the *post hoc* comparison. Quantitative data were presented as mean ± standard deviation ($n = 3$). P values of < 0.05 (*), < 0.01 (**), and < 0.001 (***) were deemed statistically significant.

3 Results and discussion

3.1 Physical characterization of PLLA/BT/collagen/FGF-18 (PBCF) composite scaffolds

3.1.1 Morphological characterization of PBCF composite scaffolds. In our previous research, it was demonstrated that ordered aligned electrostatically spun fibers promote cartilage repair.[37] Eli *et al.*[45] further established that PLLA, when spun at high rotational speeds, facilitates an ordered arrangement of fibers and can generate a significant electrical output. The utilization of PLLA with a high-voltage electrical output as a piezoelectric implant enables safe degradation and obviates the need for invasive resection procedures.

The morphology and elemental distribution of the PLLA/BT (PB) samples were analyzed using scanning electron microscopy (SEM) and transmission electron microscopy (TEM). Fig. 1a illustrates that the surface of the PLLA/BT nanofibrous membrane was devoid of beads, with the nanofibers being uniform in diameter, continuous, and aligned along the fiber direction. This uniformity suggests that BT nanoparticles (NPs) were evenly dispersed within the fiber matrix, and the arrangement of the crystalline particles was depicted. Energy-dispersive X-ray spectroscopy (EDS) confirmed the presence of BT NPs, showing a uniform distribution of carbon (C), oxygen (O), barium (Ba), and titanium (Ti) within the fiber matrix. Elemental mapping images further verified the uniform distribution of these elements throughout the fiber, as depicted in Fig. 1c. Additionally, SEM images revealed that the PLLA/BT nanofibrous membranes exhibited a porous structure reminiscent of a natural ECM, which is essential for facilitating nutrient transport and waste metabolism.[46] As shown in Fig. 1b, a 3D scaffold was engineered by combining the PB membrane with collagen, using hydrolyzed collagen as a binding agent. The PB membrane measured approximately 120 μm in thickness, whereas the collagen hydrogel layer was about 1600 μm thick, forming a tightly bonded, non-detachable composite. The collagen foam scaffolds displayed increased porosity, enhancing the diffusion of nutrients and oxygen. This increased porosity is crucial for promoting inward cell growth and tissue remodeling.[47] Therefore, we posit that the composite scaffolds not only provide a piezoelectric physiological environment conducive to cell growth but also support favorable 3D structures that enhance cell proliferation and matrix synthesis.

3.1.2 Physical characterization of PLLA/BT/collagen (PBC) composite scaffolds. Fig. 2a illustrates the absorption peaks pertinent to the analysis of chemical structures. The peak at 1751 cm^{-1} is attributed to the C=O stretching vibration, while the peaks at 1179 cm^{-1} and 1127 cm^{-1} are indicative of the C–O stretching vibrations, confirming the presence of ester groups. Additionally, the characteristic peak at 1383 cm^{-1} is identified as belonging to a methyl group, which substantiates the structural composition of PLLA. A strong absorption band at 577 cm^{-1} further corroborates the stretching vibrations of the BT nanoparticles (Ti–O).[28] Analysis conducted through Fourier transform infrared spectroscopy (FTIR) indicates that neither the electrostatic spinning process nor the introduction of BT alters the chain conformation or the crystal morphology of the PLLA substrate.

Fig. 2b presents the XRD spectrum of the PBC nanofiber membrane. The diffraction peak of BT nanoparticles, observed as a split peak at around 45°, confirms the tetragonal phase structure of the BT particles, which is known for its excellent piezoelectric properties.[48] Additionally, a distinctive peak at 16.2° was detected, indicative of a β-type PLLA phase possessing piezoelectric characteristics.[49]

The mechanical properties of the PBC nanofiber membrane were evaluated using a mechanical testing machine, which revealed exceptional mechanical strength. As shown in Fig. 2c, the initial fracture of the PBC scaffold, occurring at 19.98 MPa,
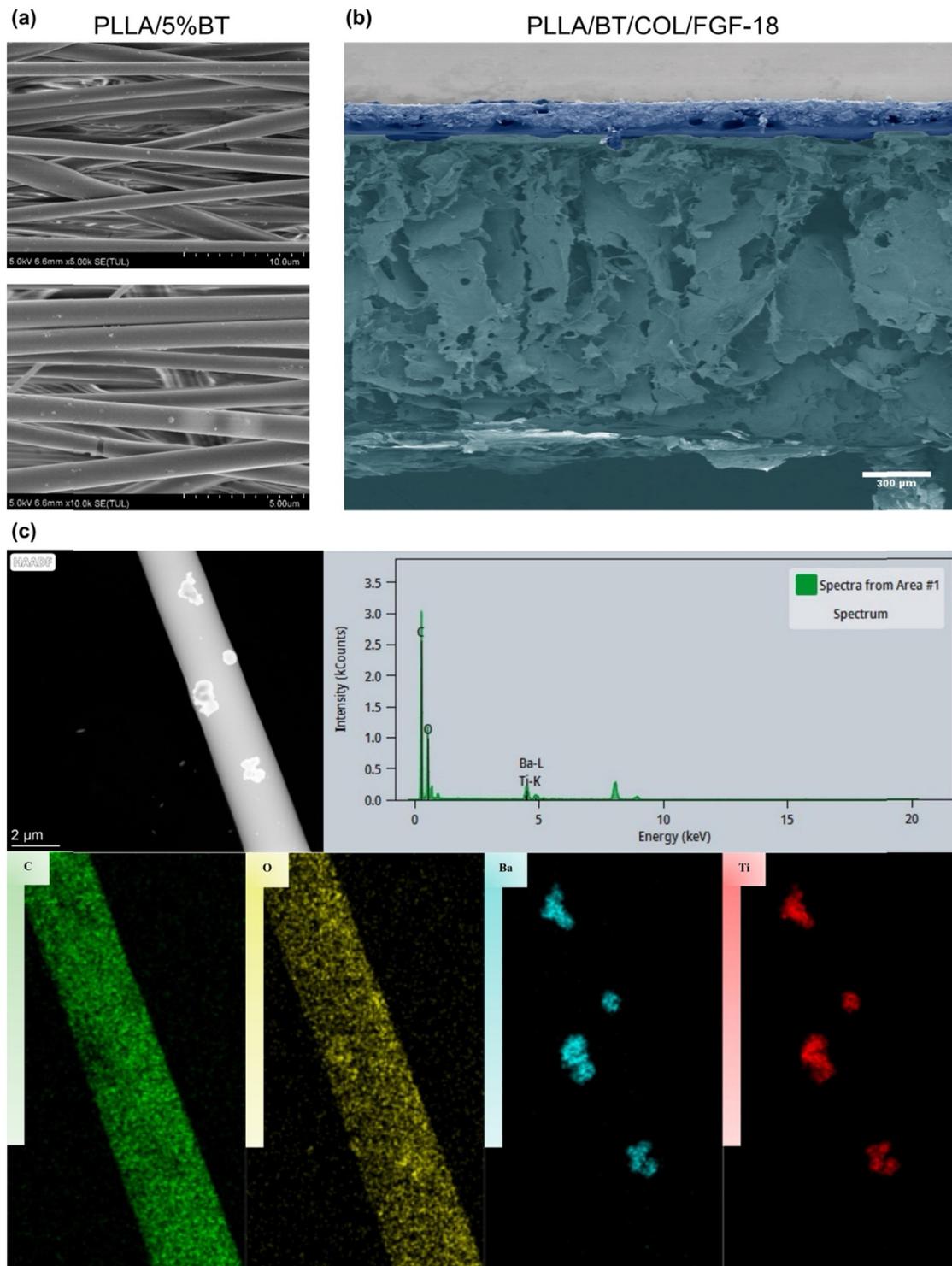
Fig. 1 (a) SEM image of electrostatically spun PLLA/BT (5%) nanofibers. (b) Cross-sectional SEM image of PBCF composite scaffolds. (c) SEM images at a high magnification and EDS spectra.

resulted from collagen failure. The second fracture, recorded at 24.02 MPa, was due to the failure of the PB nanofibrous membrane, marking the maximum load the composite could withstand. The superior mechanical properties of the PBC composites can be ascribed to several factors. Primarily, PLLA, recognized for its piezoelectric and mechanical qualities, enhances the strength of nanofiber membranes aligned along the fiber orientation compared to those with the random orientation.[35] This alignment is crucial for cartilage defect repair, which requires resilience against significant pressure and shear

This journal is © The Royal Society of Chemistry 2024

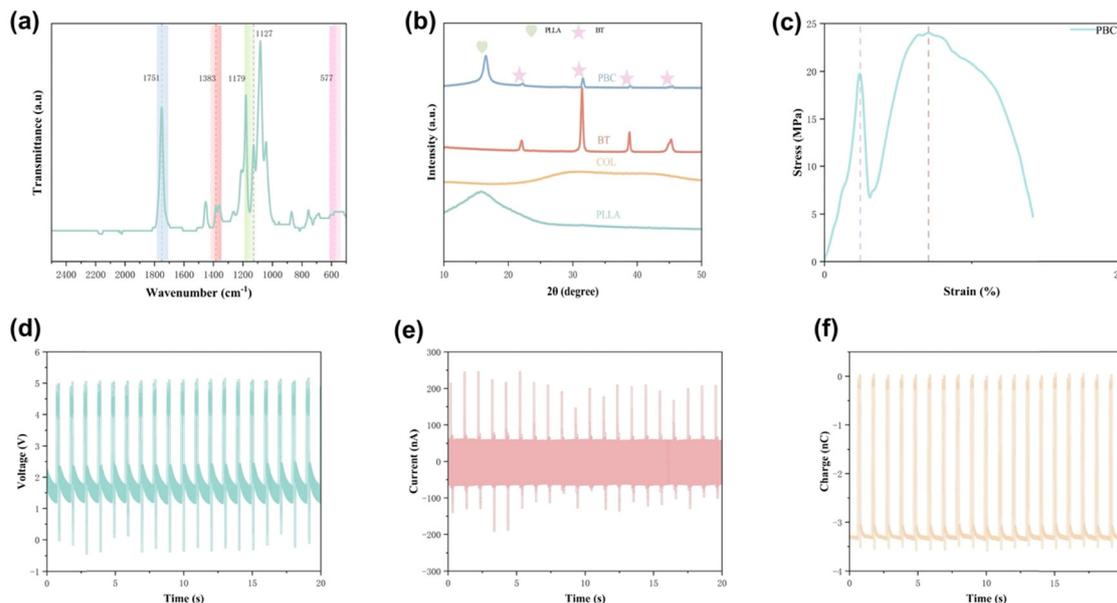*J. Mater. Chem. B*, 2024, **12**, 10416–10433 | **10421**

Fig. 2 Physical characterization of PBCF composite scaffolds: (a) FTIR result of PBC samples; (b) XRD curves of PLLA, BT, COL, and PBC samples; (c) Tensile stress–strain curves of PBC samples. The piezoelectric output of PBCF composite scaffolds: (d) the output voltage, (e) the short-circuit current, and (f) the output charge of the PBCF scaffolds.

forces. Additionally, dehydrated collagen, known for its increased mechanical strength, contributes to this robustness due to tighter molecular packing.[50] After freeze-drying, the PBCF scaffolds exhibited increased brittleness and significantly enhanced the mechanical properties, outperforming those of the PB nanofiber membranes, as shown in Fig. S4a (ESI†). Collectively, the PBC scaffolds not only demonstrate excellent mechanical properties but also meet the biomechanical demands of natural cartilage tissues, with physical tensile properties ranging from 0.3 to 10 MPa.[51]

3.1.3 The piezoelectric output of PBC composite scaffolds. To evaluate the piezoelectric output of the PBC scaffolds under external forces, the voltage, current, and charge outputs were measured using an electrostatic meter. Fig. 2d displays the open-circuit voltage and current as approximately 5 V and 200 µA, respectively. A significant increase in the piezoelectric output of the PLLA nanofiber membrane was noted (Fig. S2, ESI†), which can be attributed to the high-voltage electrical properties of the BT nanoparticles.[52] The piezoelectric characteristics of the electrostatically spun PB nanofiber films were investigated using PFM, as shown in Fig. 3a and b. The films demonstrated pronounced piezoelectric properties with a surface potential of 1.3 mV. Fig. 3c illustrates that the phase and displacement amplitude responses of the PB fibers exhibited the characteristic butterfly curve and hysteresis phenomenon, indicative of piezoelectric materials.[53] Additionally, Fig. 3d reveals that the fiber orientation angle of the PB fiber membrane was precisely aligned along the electrostatic spinning direction,[54] with an average deviation angle of approximately $11.51° \pm 6.85°$.

3.1.4 Loading and release of FGF-18. Given that composite scaffolds necessitate ultrasound (US) stimulation to induce piezoelectricity *in vitro*, the release of FGF-18 from collagen foam was assessed using the ELISA method. The release profiles of factors from composite scaffolds were compared under conditions with and without US stimulation. Fig. 3e and f depict this comparison: In the absence of US stimulation, approximately 18% of the loaded FGF-18 was released into the PBS on the first day. In contrast, with US stimulation, about 24% of the FGF-18 was released on the first day, representing a significant increase over the non-US-stimulated group and suggesting that US stimulation elicited a "burst" effect. In both scaffold groups, the release rate markedly decreased after more than 7 days, with the total factor release stabilizing at approximately 37% in the non-US-stimulated group and 44% in the sonicated group. The enhanced release in the sonicated group underscores the complex interplay between US and nanoparticles in modulating the drug release kinetics of nanostructured films, as noted in previous studies by Vannozzi et al.[55] These observations warrant further exploration of the underlying mechanical and electrical mechanisms involved.

3.2 In vitro study of PBCF composite scaffolds

3.2.1 Chondrocyte proliferation in the PBCF composite scaffolds. Biocompatibility testing of PBC and PBCF scaffolds was conducted using *in vitro* cultured articular chondrocytes. Previous research demonstrated that articular chondrocytes could proliferate steadily under US stimulation at a power of 200 W, without undergoing apoptosis due to excessive power (Fig. S4b, ESI†). Fig. 4a displays the results from the cell counting kit-8 (CCK-8) for the PBC and PBCF scaffold groups, both with and without US stimulation, over periods of 3, 5, and 7 days. Optical density (OD) values were measured at 480 nm using an enzyme marker. By the third day, a statistically significant increase in chondrocyte proliferation was noted in
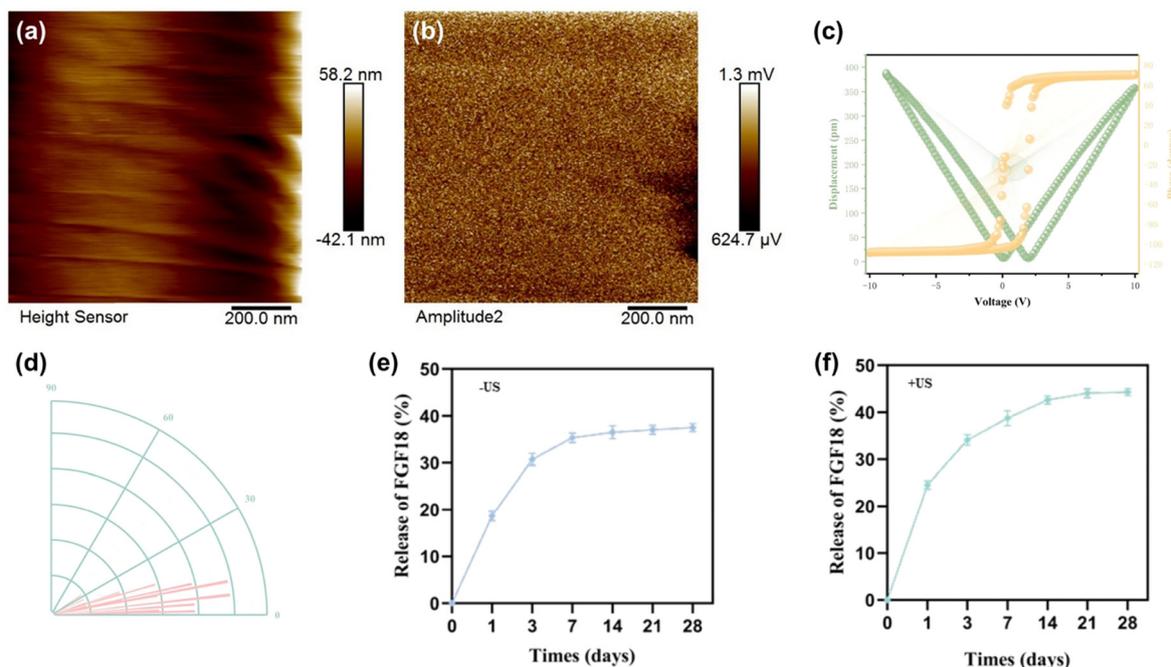
10422 | J. Mater. Chem. B, 2024, **12**, 10416–10433

This journal is © The Royal Society of Chemistry 2024

Fig. 3 (a) and (b) PFM graphs of PB nanofiber membranes. (c) PFM phase and amplitude graphs of electrospun PB nanofibers. (d) Fiber orientation deviation angle. *In vitro* FGF-18 release tests (e) without and (f) with US stimulation.

the PBCF + US group compared to the PBC and PBC + US groups. This increase was attributed to US stimulation, which facilitated the early release of FGF-18 activating factor from the PBCF scaffold, thereby promoting chondrocyte proliferation. Despite US stimulation also promoting chondrocyte proliferation, the extent of proliferation in the PBC group was greater than that in the PBC + US group at this time, indicating that US stimulation did not significantly enhance chondrocyte proliferation at this stage. Subsequent statistical analysis showed significant differences in OD values between the PBCF + US group and the other groups ($p < 0.001$). The role of FGF-18 in chondrocyte proliferation is well-established, with chondrocytes and osteoblasts serving as the primary target cells. FGF-18 is known to facilitate chondrocyte proliferation and matrix production.[56,57] As noted, encapsulation of FGF-18 within collagen leads to early factor release, significantly enhancing chondrocyte proliferation in the initial stages. Moreover, cartilage exhibits a heightened response to electrical stimulation compared to other tissues, with documented enhancement of chondrocyte proliferation due to electrical stimulation.[9,58] Chondrocytes cultured on composite scaffolds were subjected to daily US stimulation for 20 minutes from day 1 to day 7, inducing piezoelectric generation and synergizing with the FGF-18 to further promote chondrocyte growth.

To further explore the cytocompatibility of the materials, live–dead cell staining was utilized to assess the cell viability. Articular chondrocytes were cultured on PBC and PBCF composite scaffolds and subjected to 200 W ultrasonic stimulation for three days. As depicted in Fig. 4c, the live–dead staining experiments showed that articular chondrocytes adhered to and proliferated on both types of scaffolds. Both the PBC and PBCF groups, regardless of ultrasonic stimulation, demonstrated excellent biocompatibility with minimal cell death (indicated by red staining) and preserved the cell morphology and structure. The survival rates were significantly higher in the PBCF and PBCF + US groups compared to the PBC group without piezoelectricity and the PBC + US group. A significantly greater number of proliferating chondrocytes was observed in the PBCF + US group relative to the PBC + US group, suggesting that the release of the FGF-18 promoted chondrocyte proliferation, corroborating the cell counting results described previously. The ratio of live cell area to dead cell area, illustrated in Fig. 4b, showed a lower proportion of dead cells across all groups, with the PBCF + US group exhibiting a notably smaller dead cell area compared to the PBC group.

The chondrocyte growth morphology, characterized by actin (green) and nuclei (blue), was assessed through 4′,6-diamidino-2-phenylindole (DAPI) and F-actin staining in PBC, PBCF, and their respective US stimulation groups. Fig. 4d illustrates that chondrocytes were uniformly dispersed and well-aligned on the scaffold surfaces across all groups, exhibiting a good growth status. Specifically, the actin skeletons were aligned parallel to the nanofiber axes on the surfaces of the PB membranes, and cells appeared elongated, mimicking the orientation of the nanofibers. This alignment was consistent with findings from previous studies,[8] which have demonstrated that nanofiber topology significantly influences cell orientation, proliferation, and the augmentation of the cartilage matrix content.[59] The favorable condition of all cells across the scaffold groups underscores their excellent biocompatibility and potential as piezoelectric materials for cartilage repair.

3.2.2 Determination of collagen and hydroxyproline contents. Collagen and glycosaminoglycans (GAG), vital constituents of the

This journal is © The Royal Society of Chemistry 2024

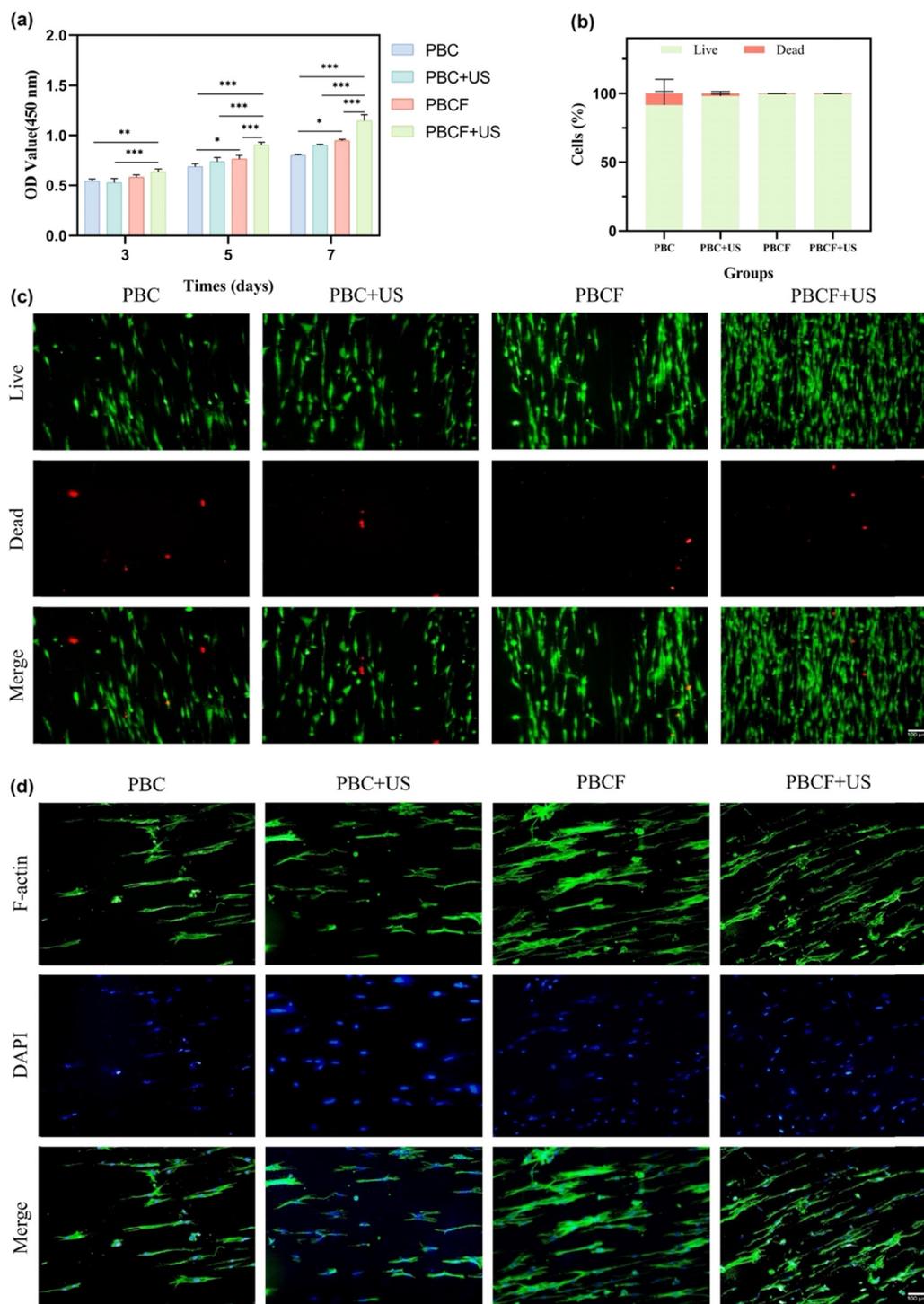*J. Mater. Chem. B*, 2024, **12**, 10416–10433 | **10423**

Fig. 4 *In vitro* proliferation in scaffolds. (a) Cell proliferation histograms after culture for 3, 5, and 7 days (*$p < 0.05$, **$p < 0.01$, and ***$p < 0.001$). (b) The proportion of live−dead cell areas. (c) Live/dead staining images after 3 days of co-culture. (d) F-actin/DAPI staining images on different groups (blue: nucleus; green: actin network) ($n = 4$, scale bar = 100 um).

ECM in articular cartilage, were analyzed in terms of their production within PBC and PBCF scaffolds, both with and without US stimulation. Production levels of GAG and hydroxyproline (HYP) were normalized against the DNA content. Fig. 5a displays the findings from the DNA assay. Initially, no significant variations in the DNA content were noted among the groups during the first three days. However, by days 7 and 14, the DNA content in the PBCF + US group significantly exceeded that of the other groups, with the difference on day 14 surpassing that observed on day 7. While no notable differences in GAG and

10424 | *J. Mater. Chem. B*, 2024, **12**, 10416–10433

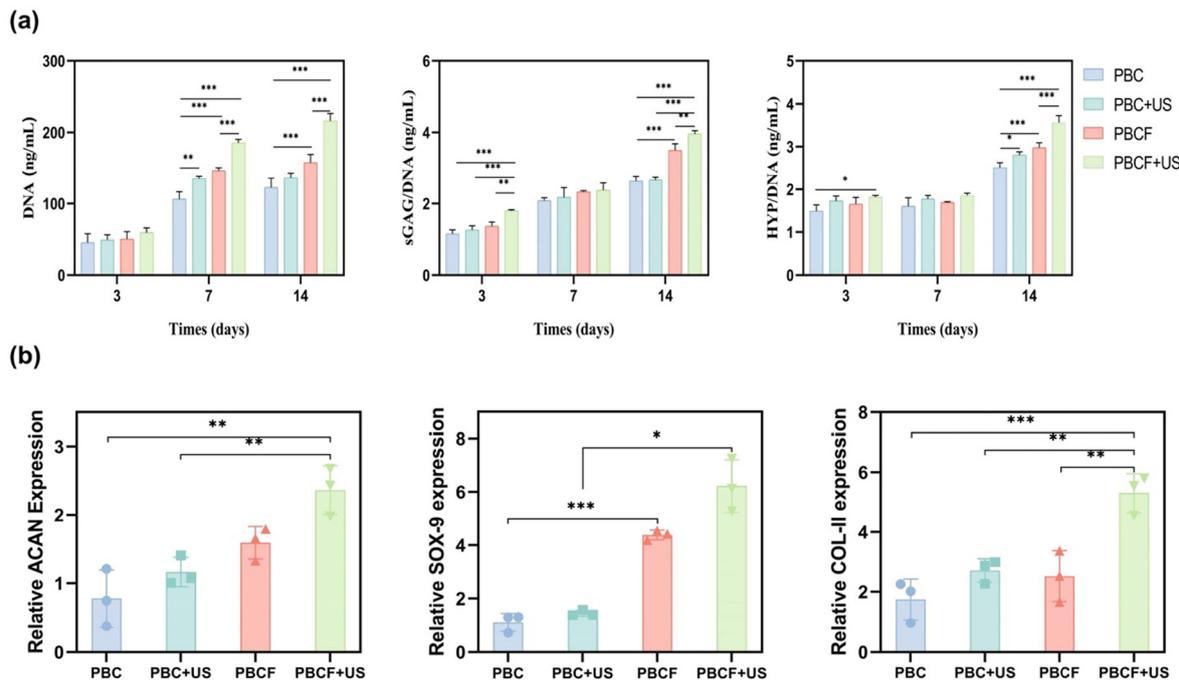This journal is © The Royal Society of Chemistry 2024

Fig. 5 Determination of collagen and hydroxyproline contents and analysis of gene expression results. (a) DNA content of articular chondrocytes in different groups after 3, 7, and 14 days of co-culture; GAG and hydroxyproline production by articular chondrocytes in different groups after 3,7, and 14 days of co-culture. (b) Expression of *ACAN*, *SOX-9*, and *COL-II* genes in articular chondrocytes on different groups after 14 days of co-culture. (n = 3, *$p < 0.05$,**$p < 0.01$ and ***$p < 0.001$).

HYP deposition were found between the PBCF + US group and others on day 7, the deposition rates on this day remained higher than those recorded on day 3. Furthermore, GAG and HYP levels in the PBCF + US group were significantly greater than those in other groups on both days 3 and 14, indicating statistically significant differences.

The PBCF + US group exhibited a superior generation of the cartilage ECM, a result attributed to multiple factors. Initially, ECM secretion in the PBC group consistently increased over time, illustrating the scaffolds' effectiveness in facilitating cartilage ECM secretion.[60,61] The morphological characteristics of the material, including its chemical composition, wettability, and microstructure, significantly influenced cellular ECM secretion. Surface pores within the fibrous scaffolds were deemed essential for enhancing GAG and HYP formation. By day 14, the PBC + US group demonstrated increased HYP generation relative to the PBC group, signifying enhanced ECM production. US stimulation has been shown to activate genes or receptors that mediate the aggregation of mesenchymal stem cells (MSCs) and cartilage formation, while also promoting chondrogenic differentiation through cascade signaling.[62–64] Moreover, by day 14, the PBCF group displayed superior pro-chondrogenic ECM generation compared to the PBC group. Studies by Muller *et al.*[65] reported a significant increase in the chondrocyte count and GAG content following *in vitro* FGF-18 treatment using bovine chondrocytes. Similarly, Ellsworth *et al.* confirmed that FGF-18 effectively stimulated chondrocyte proliferation and enhanced GAG expression. Additionally, it has been established that FGF-18 selectively activates fibroblast growth factor receptor 3 (FGFR3) in cartilage

and chondrocytes; this activation plays a critical role in the development of cartilage and bone, promoting both chondrocyte proliferation and extracellular matrix deposition in monolayer cell cultures.[66]

In summary, the superior performance of the PBCF + US group in promoting chondrocyte cytoplasmic matrix deposition can be attributed to the scaffold material's excellent biocompatibility and the dual promotional effects of piezoelectricity combined with the active FGF-18 on chondrocyte proliferation and matrix generation.

3.2.3   Analysis of gene expression results. After 14 days of co-culture, the results of chondrocyte-related gene expression (Fig. 5b) demonstrated that under ultrasound stimulation, PBCF 3D composite scaffolds exhibited higher expression levels of chondrocyte-related genes, including aggregated protein (*ACAN*), recombinant sex-determining region Y box protein-9 (*SOX-9*), and collagen type II (*COL-II*), compared to the PBC, PBC + US, and PBCF groups. These differences were statistically significant, with the exception of *ACAN* gene expression. *ACAN*, which encodes aggrecan – a key protein synthesized by chondrocytes – was expressed notably higher in the PBCF + US group than in the PBC group,[67] and this disparity was statistically significant. Such findings underscore the synergistic effects of piezoelectric stimulation and the FGF-18 in enhancing chondrocyte activity and promoting aggrecan expression. A significant increase in *SOX-9* expression in the PBCF + US group, compared to that in the PBC group, indicated a superior capacity for enhancing extracellular matrix secretion by chondrocytes. *SOX-9* is crucial for regulating the expression of genes

This journal is © The Royal Society of Chemistry 2024

J. Mater. Chem. B, 2024, **12**, 10416–10433 | **10425**

responsible for encoding type II collagen and proteoglycan aggregation proteins within the ECM.[68] As a major component of articular cartilage, type II collagen levels typically increase with collagen maturation,[69] and notably, these levels were observed to increase more prominently under ultrasound stimulation in the presence of PBCF compared to other groups.

In summary, significantly higher levels of *ACAN*, *SOX-9*, and *COL-II* gene expression were exhibited by the PBCF + US group compared to the PBC group. This disparity is attributable to two main factors. Firstly, studies by Gigout *et al.* demonstrated that FGF-18 *in vitro* enhances the type II collagen content and the extracellular matrix volume, whereas Shimoaka *et al.* found that FGF-18 promotes cartilage matrix formation by mitigating chondrocyte differentiation.[68,70] These studies suggest a superior ability of FGF-18 to promote chondrogenic matrix formation and chondrocyte proliferation *in vitro*. Secondly, piezoelectric stimulation has been shown to be crucial in enhancing the expression of cartilage-related genes and ECM synthesis. Electrical stimulation effectively promotes the expression of the bone morphogenetic protein (BMP), initiating cartilage formation and subsequently driving mRNA expression for *COL-II*, *ACAN*, and *SOX-9*.[13] McCullen *et al.*[71] demonstrated that piezoelectric stimulation decreases type I collagen levels while increasing the expression of cartilage-forming markers such as *COL-II*, *ACAN*, and *SOX-9*, thus facilitating cartilage matrix formation. Compared with either the FGF-18 alone or the piezoelectric stimulation alone, the synergistic effect of combining FGF-18 with piezoelectric stimulation plays a significant role in promoting chondrocyte proliferation and matrix formation.[71]

3.3 *In vivo* study of PBCF composite scaffold-induced cartilage defect repair in rabbits

Materials characterization and *in vitro* cellular experiments were followed by the use of a rabbit model to assess the reparative effects of PBCF scaffolds on critical-size osteochondral defects. Motor stimulation-induced piezoelectric generation was utilized. Osteochondral defects were surgically created in the femoral condyles of the rabbits using a mill drill. Before the surgical intervention, all rabbits underwent one month of treadmill exercise training to acclimate them to the activity. Thirty-six rabbits were randomly assigned into six groups: defect only, PBC, PBCF, defect + exercise, PBC + exercise, and PBCF + exercise, with three legs per group (n = 3). Following surgery, the rabbits were administered daily antibiotics for three days, with no adverse reactions observed until euthanasia. A postoperative rest period of two weeks was allowed for organic recovery before resuming exercise training. It has been demonstrated in previous studies that exercise training within two weeks post-cartilage injury exacerbates the damage.[72] The complete animal experimental procedure is depicted in Fig. 6a.

Treadmill training was conducted for 20 minutes per day, five days a week, for durations of either one or two months (Video S1, ESI†). This training regimen was designed to induce joint loading during movement, thereby promoting piezoelectric effects within the scaffold. The chosen duration is supported by prior studies, which suggest that 15 minutes of daily exercise in conjunction with poly(lactic-*co*-glycolic acid) (PLGA) scaffolds enhances cartilage regeneration.[73] Furthermore, Liu *et al.*[11] reported that extended durations of exercise lead to increased fatigue in rabbits.

3.3.1 Macroscopic analysis. Knee joints from rabbits were harvested at two time points (1 and 2 months) and subjected to macroscopic analysis of cartilage repair, as illustrated in Fig. 6b. Initially, the macroscopic evaluation of the harvested cartilage revealed that, after two months *in vivo*, the control group, the PBCF group, the PBC scaffold, and its associated exercise group displayed less repair of cartilage and subchondral bone tissues compared to the PBCF + exercise group. In the control group, a pronounced depression at the defect site was still evident. The PBC scaffold group showed clear demarcations between the defect and surrounding tissues, with minimal cartilage formation noted. Both the PBC + exercise and PBCF groups exhibited noticeable depressions at the defect site, with minor color variations from the surrounding tissues, indicative of partial cartilage formation. Conversely, the exercise group displayed no significant surface depression at the defect site; the boundary had nearly vanished, and the newly formed cartilage appeared smooth and white, blending seamlessly with adjacent tissues. The color of this new tissue closely matched that of the native tissue, suggesting a higher level of defect repair. These observations suggest that piezoelectric stimulation, in conjunction with FGF-18, enhances cartilage defect repair, corroborating the results from *in vitro* cellular experiments.

Fig. 6d presents the International Cartilage Repair Society (ICRS) system scores for specimens at 1 and 2 months, offering a quantitative evaluation of cartilage defect repair across the groups. The PBCF + exercise group consistently recorded significantly higher scores than the control group, the PBC group, and its exercise counterpart at both evaluated time points, indicating enhanced cartilage regeneration. Furthermore, scores at 2 months for the PBCF + exercise group were significantly higher than those at 1 month, demonstrating marked improvement over time, with a statistically significant difference (P < 0.01).

3.3.2 Imaging evaluation. To further assess the morphological changes in cartilage, micro-MRI scanning was employed to examine the knee joint. This technique offers high resolution of soft tissues and is sensitive to variations in the water content of the tissue components, thereby providing a superior evaluation of cartilage damage repair.[74] As depicted in Fig. 6c, MRI imaging within the first-month post-repair revealed uneven cartilage surfaces across all groups. By the second month, the PBCF + exercise group demonstrated a smoother and more continuous cartilage surface, exhibiting lower signal intensity compared to both the PBC group and its exercise counterpart. This enhancement in cartilage regeneration was statistically significant (P < 0.05), as evidenced by the Henderson scores shown in Fig. 6e. Despite these improvements, the PBCF + exercise group's repair was significantly superior only to the blank group, with no statistically significant differences noted when compared

10426 | *J. Mater. Chem. B*, 2024, **12**, 10416–10433

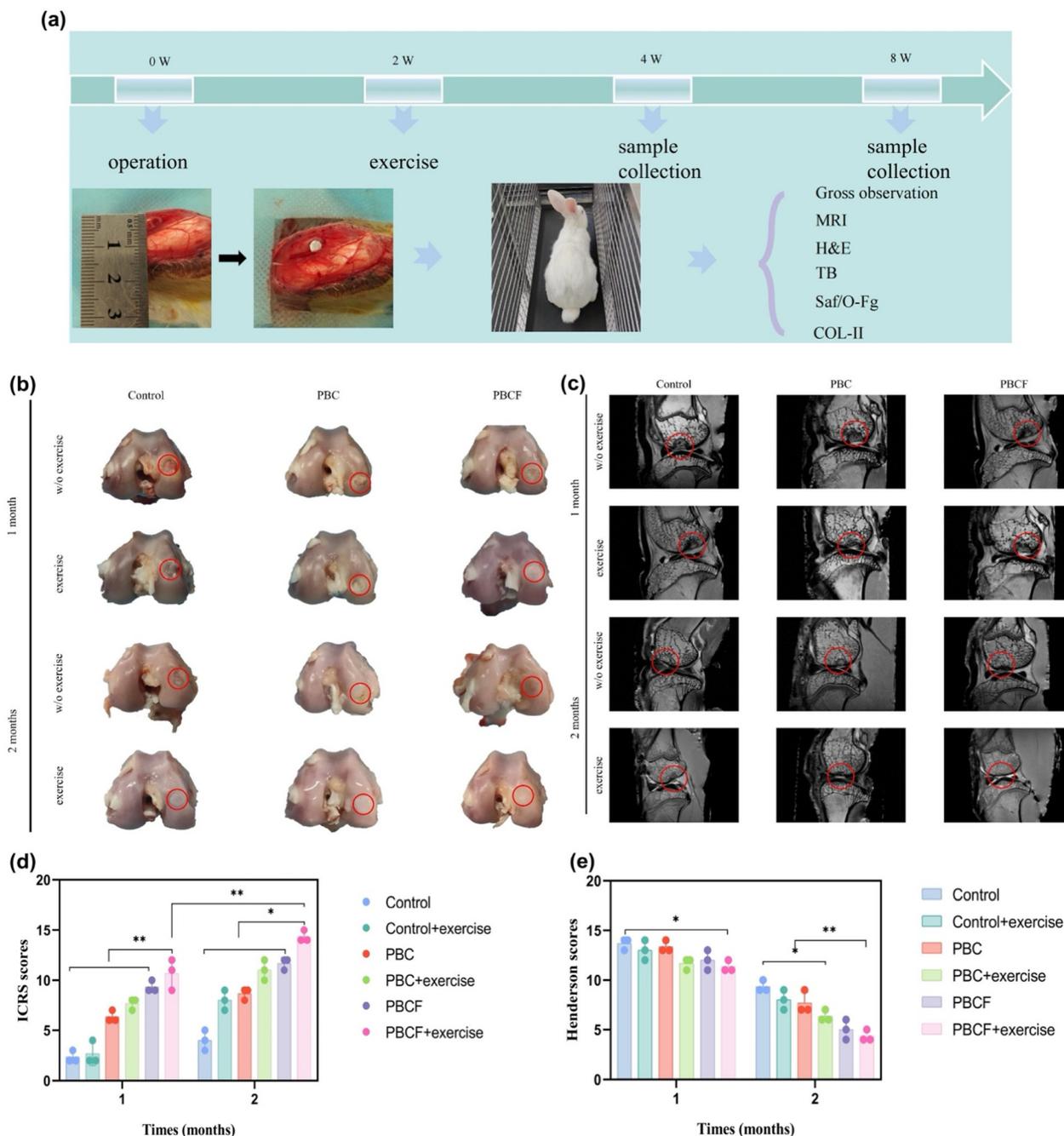This journal is © The Royal Society of Chemistry 2024

Fig. 6 Scaffolds induced cartilage defect repair in the rabbit model. (a) A scheme of PBCF composite scaffolds for repair of articular cartilage defects in rabbits. (b) Gross observations of cartilage integrity in the knee joint at 1 and 2 months after PBCF composite scaffold implantation. (c) MRI images of rabbit knees. Red circles mark the sites of initial cartilage defects. (d) ICRS score grading of the cartilage defect. (e) Henderson scores of MRI. Data are presented as the mean $\pm$ SD ($n = 3$. *$p < 0.05$ and **$p < 0.01$ analyzed using ANOVA with Tukey's multiple comparison test).

to the other groups. It is noteworthy that, following surgery, all rabbits underwent a compulsory two-week postoperative rehabilitation phase during which exercise was prohibited, precluding piezoelectric generation through movement. Nevertheless, the sustained release of FGF-18 during this period also played a crucial role in promoting cartilage repair. Starting from the third week, a co-promotion strategy involving exercise-induced piezoelectric generation combined with FGF-18 was initiated.

After eight weeks, the cartilage healing observed in the PBC + exercise group was notably superior compared to both the PBCF + exercise and blank groups. The PBCF + exercise group exhibited a smoother, curved, and continuous cartilage surface on MRI, in contrast to the PBCF, PBC, control, and their respective exercise groups. However, the PBC + exercise group displayed a slightly concave surface. According to the Henderson score, the PBCF + exercise group scored significantly lower

than the control, PBC, and its exercise group ($P < 0.01$), indicating improved cartilage regeneration compared to the control group. Remarkably, there was no significant difference between the PBCF + exercise and the PBC + exercise groups, suggesting limitations in the precision of the Henderson scoring system for the detailed assessment of cartilage repair.

3.3.3 Histology and immunohistochemical analysis. Cartilage repair was assessed using a variety of immunohistochemical staining methods. For histological evaluation, hematoxylin and eosin (H&E), safranin O-fast green (Saf O-Fg), and toluidine blue staining were employed to determine the extent and quality of the repair. Significant differences in H&E staining results were observed between the groups at 1 and 2 months postoperatively, following exercise regimens or the absence thereof (Fig. 7a). In the control group, a new fibrous tissue was found to fill a small portion of the defects at both time points, with no visible cartilage
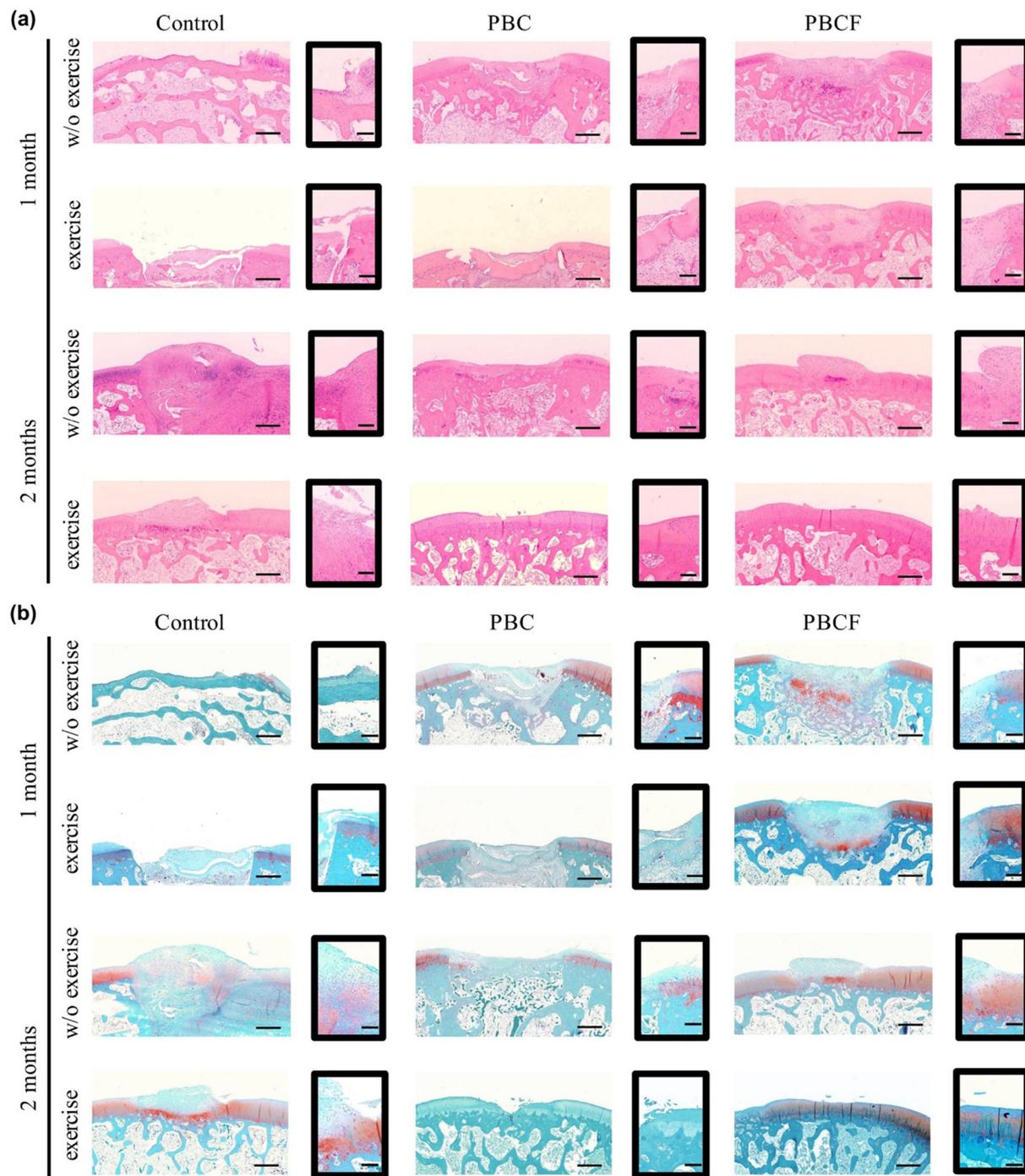

Fig. 7 (a) H&E staining to assess articular cartilage regeneration (n = 3 knees for each group, scale bar = 500 um). (b) Safranin O-fast green staining to assess articular cartilage regeneration (n = 3 knees for each group, scale bar = 500 um).

10428 | *J. Mater. Chem. B*, 2024, **12**, 10416–10433

This journal is © The Royal Society of Chemistry 2024

formation. In contrast, the PBC + exercise group exhibited enhanced cartilage repair by 2 months, where the distinct cartilage-like tissue was observed, albeit with very thin cartilage thickness and poor subchondral bone formation. Notably, the PBCF + exercise group demonstrated robust new cartilage

formation by 2 months postoperatively, characterized by the visible chondrocyte morphology and a smooth cartilage surface that resembled surrounding normal tissues.

The distribution of glycosaminoglycans (GAGs) within the newly formed cartilage tissue was assessed using safranin
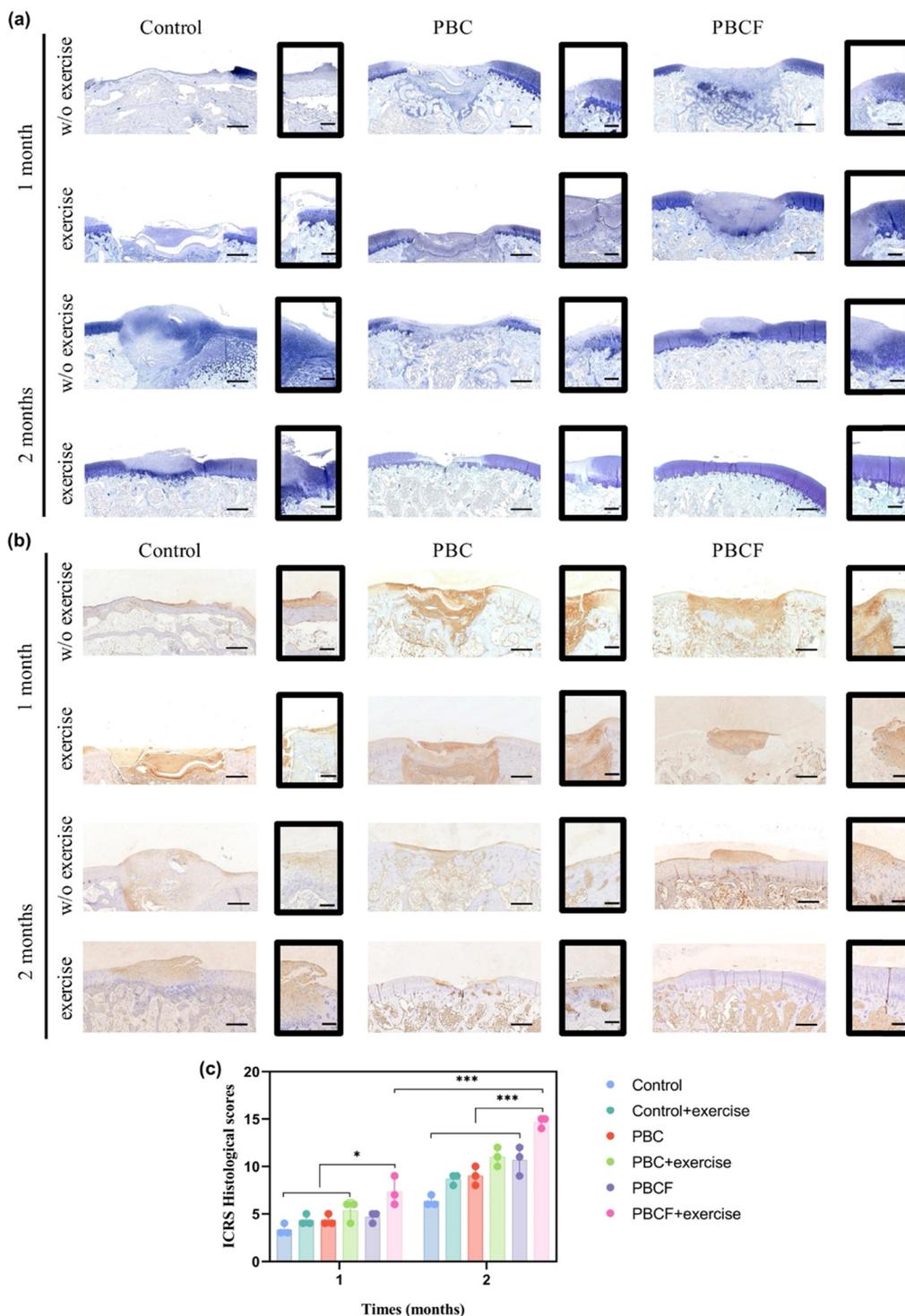

Fig. 8 (a) Toluidine blue staining to assess articular cartilage regeneration ($n = 3$ knees for each group, scale bar = 500 um). (b) Collagen II staining (IHC) to assess articular cartilage regeneration ($n = 3$ knees for each group, scale bar = 500 um). (c) ICRS histological evaluation, data are presented as the mean ± SD ($n = 3$. *$p < 0.05$ and **$p < 0.01$ analyzed using ANOVA with Tukey's multiple comparison test).

This journal is © The Royal Society of Chemistry 2024

J. Mater. Chem. B, 2024, **12**, 10416–10433 | **10429**

O-fast green (Saf O-Fg) staining, while toluidine blue staining, known for its affinity for sulfate groups, was employed to detect proteoglycans in the cartilage (Fig. 7b and 8a). At 1 month postoperatively, negligible new cartilage formation was observed in the control, PBC, and PBC + exercise groups, with a lower GAG content compared to the defect center in the PBCF + exercise group. By 2 months postoperatively, the PBCF + exercise group exhibited a significantly narrower boundary with the surrounding normal cartilage, indicative of hyaline cartilage formation. In contrast, the PBC group and its exercise counterpart displayed some new cartilage formation, yet their subchondral bone formation remained inadequate. Meanwhile, both the control group and its exercise counterpart continued to exhibit noticeable cartilage defects. Additionally, immunohistochemical staining for collagen type II (COL-II) was utilized to specifically assess cartilage tissue regeneration, as depicted in Fig. 8b. High positivity for type II collagen staining in the PBCF + exercise group suggested that the defects were rich in type II collagen and displayed a collagen fiber structure similar to that of the natural tissues. In comparison, the other groups showed minimal or no type II collagen production. Slight cartilage improvement was also observed in the PBCF and PBC scaffold groups not subjected to exercise, possibly attributable to the free movement of the rabbits, which may activate piezoelectricity to some extent, corroborating the findings of Liu et al.[11]

As depicted in Fig. 8c, the histological scores demonstrated significantly superior cartilage defect repair in the PBCF + exercise group compared to the control, PBCF, PBC, and PBC + exercise groups, with notable differences observed at both one and two months ($p < 0.05$ at 1 month; $p < 0.001$ at 2 months). Furthermore, histological scores for cartilage repair in the PBCF + exercise group were significantly higher at 2 months than at 1 month ($p < 0.001$). Although limited subchondral bone and chondrocyte production occurred at the defect sites in the PBC + exercise and PBCF groups, these components exhibited poor integration. The combination of PBCF composite scaffolds with exercise-stimulated synergistic factor release led to smoother defect planes, enhanced regeneration of the hyaline cartilage matrix, increased cell viability, and improved cellular distribution, culminating in enhanced histologic scores.

Liu et al.[11] were pioneers in implanting PLLA nanofiber piezoelectric scaffolds into cartilage defects in rabbits, proposing for the first time the combination of biomechanical activity with piezoelectric materials to foster cartilage repair. Their study required a one-month rest period for rabbits post-surgery before initiating running exercises. In contrast, our study found that rabbits could begin running exercises independently after only two weeks of the post-surgical test, based on two primary considerations: firstly, prior research suggests that exercising within two weeks post-surgery may exacerbate cartilage damage;[72] secondly, during the initial two weeks, rabbits generally lack the capability to exercise or generate piezoelectricity. Nonetheless, the slow release of FGF-18 in vivo compensates for the absence of piezoelectricity in facilitating cartilage repair during this period. Vinikoor et al.[27]

further advanced the field by implanting a novel piezoelectric hydrogel into rabbits, opting for direct ultrasound stimulation in vitro to promote cartilage repair. Conversely, our approach leveraged the natural piezoelectricity generated through the biomechanical activities of the rabbits. This decision was influenced by several factors: firstly, ultrasound stimulation is labor-intensive and its effects cannot be standardized accurately; secondly, exercise has been shown to exert an anti-inflammatory effect by creating an anti-inflammatory microenvironment during loading and unloading exercises, whereas a lack of physical activity increases the risk of inflammation.[75–77]

In conclusion, the activation of critical size defects in osteochondral cartilage by ultrasound led to enhanced subchondral bone formation and significant improvement in the structure of hyaline cartilage, which closely resembled natural cartilage. These studies collectively suggest that the in vivo application of piezoelectric scaffolds for cartilage defect repair, whether through self-motion or ultrasound stimulation, significantly enhances cartilage repair by inducing the piezoelectric stimulation of the scaffolds. Furthermore, in the in vivo repair of articular cartilage defects, the active factor FGF-18 has proven effective in promoting chondrocyte proliferation and in facilitating the production of a clearer and more transparent extracellular matrix. Additionally, FGF-18 influences the metabolism of articular cartilage by enhancing the metabolic activity and promoting the production of type II collagen.[78] FGF-18 also contributes to the increased cartilage thickness while minimizing cartilage loss.[24] The combination of piezoelectric stimulation with active biological factors synergistically enhances cartilage repair, leading to improved outcomes in the repair of cartilage defects. Moreover, this approach significantly reduces the overall time required for cartilage repair, thereby facilitating more effective and rapid cartilage regeneration.

4 Conclusions

The development of a piezoelectric composite scaffold, composed of polylactic acid (PLLA), barium titanate (BT), collagen, and fibroblast growth factor-18 (FGF-18), has yielded a material with exceptional mechanical and piezoelectric properties. This PLLA/BT/collagen/FGF-18 (PBCF) composite scaffold, characterized by a high mechanical strength of 24 kPa and a piezoelectric output of up to approximately 5 V, demonstrates significant potential for cartilage repair. In vitro studies have confirmed its excellent biocompatibility, which facilitates chondrocyte proliferation, enhances glycosaminoglycan production, and promotes regeneration of the ECM. Additionally, these studies have observed a notable upregulation in the expression of cartilage-specific genes. And, in vivo experiments focusing on the repair of cartilage defects have shown that the PBCF composite scaffold accelerates cartilage tissue repair, especially when combined with exercise-induced stimulation, thereby highlighting its viability as a treatment option for patients with superficial cartilage defects.

10430 | J. Mater. Chem. B, 2024, **12**, 10416–10433

This journal is © The Royal Society of Chemistry 2024

Author contributions

Bowen Xie: data curation, formal analysis, investigation, methodology, visualization, writing – original draft, and writing – review and editing. Hebin Ma: data curation, formal analysis, investigation, methodology, visualization, writing – original draft, and writing – review and editing. Fengyuan Yang: data curation, formal analysis, investigation, methodology, visualization, writing – original draft, and writing – review and editing. Hongguang Chen: data curation, formal analysis, investigation, methodology, visualization, writing – original draft, and writing – review and editing. Ya'nan Guo: methodology, supervision, validation, and writing – review and editing. Hongxing Zhang: methodology, supervision, validation, and writing – review and editing. Tengfei Li: formal analysis, validation, and writing – review and editing. Xiaogang Huang: formal analysis, validation, and writing – review and editing. Yantao Zhao: conceptualization, funding acquisition, methodology, project administration, supervision, and writing – review and editing. Xiaojie Li: conceptualization, funding acquisition, methodology, project administration, supervision, and writing – review and editing. Junjie Du: conceptualization, funding acquisition, methodology, project administration, supervision, and writing – review and editing. All authors read and approved the final manuscript.

Data availability

The data that support the findings of this study are available upon request from the corresponding author, [Junjie Du].

Conflicts of interest

There are no conflicts of interest to declare.

Acknowledgements

Notes and references

1 A. J. Sophia Fox, A. Bedi and S. A. Rodeo, *Sports Health*, 2009, **1**, 461–468.

2 J. A. Buckwalter and H. J. Mankin, *Arthritis Rheum.*, 1998, **41**, 1331–1342.

3 S. L. Vega, M. Y. Kwon and J. A. Burdick, *Eur. Cells Mater.*, 2017, **33**, 59–75.

4 B. R. da Costa, T. V. Pereira, P. Saadat, M. Rudnicki, S. M. Iskander, N. S. Bodmer, P. Bobos, L. Gao, H. D. Kiyomoto, T. Montezuma, M. O. Almeida, P. S. Cheng, C. A. Hincapié, R. Hari, A. J. Sutton, P. Tugwell, G. A. Hawker and P. Jüni, *BMJ*, 2021, **375**, n2321.

5 E. B. Hunziker, K. Lippuner, M. J. Keel and N. Shintani, *Osteoarthritis Cartilage*, 2015, **23**, 334–350.

6 R. S. Tuan, A. F. Chen and B. A. Klatt, *J. Am. Acad. Orthop. Surg.*, 2013, **21**, 303–311.

7 D. Kai, M. P. Prabhakaran, G. Jin and S. Ramakrishna, *J. Biomed. Mater. Res., Part B*, 2011, **98**, 379–386.

8 B. Xie, F. Yang, H. Chen, H. Zhang, H. Ma, T. Li, Z. Chen, J. Li, X. Li and J. Du, *Front. Mater.*, 2023, **10**.

9 L. Massari, F. Benazzo, M. De Mattei, S. Setti and M. Fini, *J. Bone Jt. Surg., Am.*, 2007, **89**(3), 152–161.

10 B. Hiemer, M. Krogull, T. Bender, J. Ziebart, S. Krueger, R. Bader and A. Jonitz-Heincke, *Mol. Med. Rep.*, 2018, **18**, 2133–2141.

11 Y. Liu, G. Dzidotor, T. T. Le, T. Vinikoor, K. Morgan, E. J. Curry, R. Das, A. McClinton, E. Eisenberg, L. N. Apuzzo, K. T. M. Tran, P. Prasad, T. J. Flanagan, S. W. Lee, H. M. Kan, M. T. Chorsi, K. W. H. Lo, C. T. Laurencin and T. D. Nguyen, *Sci. Transl. Med.*, 2022, **14**, eabi7282.

12 S. D. Cook, S. L. Salkeld, L. S. Popich-Patron, J. P. Ryaby, D. G. Jones and R. L. Barrack, *Clin. Orthop. Relat. Res.*, 2001, S231–S243, DOI: 10.1097/00003086-200110001-00022.

13 H. J. Kwon, G. S. Lee and H. Chun, *Sci. Rep.*, 2016, **6**, 39302.

14 Z. Liu, X. Wan, Z. L. Wang and L. Li, *Adv. Mater.*, 2021, **33**, e2007429.

15 C. T. Brighton, W. Wang, R. Seldes, G. Zhang and S. R. Pollack, *J. Bone Jt. Surg., Am.*, 2001, **83**, 1514–1523.

16 R. K. Aaron and D. M. Ciombor, *J. Cell. Biochem.*, 1993, **52**, 42–46.

17 L. P. da Silva, S. C. Kundu, R. L. Reis and V. M. Correlo, *Trends Biotechnol.*, 2020, **38**, 24–49.

18 R. Nuccitelli, *Radiat. Prot. Dosim.*, 2003, **106**, 375–383.

19 T. Zheng, H. Wu, Y. Yuan, X. Lv, Q. Li, T.-L. Men, C. Zhao, D.-Q. Xiao, J. Wu, K. Wang, J. Li, Y. Gu, J. Zhu and S. J. Pennycook, *Energy Environ. Sci.*, 2017, **10**, 528–537.

20 Y. Tang, C. Wu, Z. Wu, L. Hu, W. Zhang and K. Zhao, *Sci. Rep.*, 2017, **7**, 43360.

21 X. Dai, X. Yao, W. Zhang, H. Cui, Y. Ren, J. Deng and X. Zhang, *Int. J. Nanomed.*, 2022, **17**, 4339–4353.

22 D. Davidson, A. Blanc, D. Filion, H. Wang, P. Plut, G. Pfeffer, M. D. Buschmann and J. E. Henderson, *J. Biol. Chem.*, 2005, **280**, 20509–20515.

23 Y. Wang, T. Yang, Y. Liu, W. Zhao, Z. Zhang, M. Lu and W. Zhang, *Int. J. Mol. Sci.*, 2017, 18.

24 J. L. Ellsworth, J. Berry, T. Bukowski, J. Claus, A. Feldhaus, S. Holderman, M. S. Holdren, K. D. Lum, E. E. Moore, F. Raymond, H. Ren, P. Shea, C. Sprecher, H. Storey, D. L. Thompson, K. Waggie, L. Yao, R. J. Fernandes, D. R. Eyre and S. D. Hughes, *Osteoarthritis Cartilage*, 2002, **10**, 308–320.

25 Y. R. Yun, J. E. Won, E. Jeon, S. Lee, W. Kang, H. Jo, J. H. Jang, U. S. Shin and H. W. Kim, *J. Tissue Eng.*, 2010, **2010**, 218142.

26 E. E. Moore, A. M. Bendele, D. L. Thompson, A. Littau, K. S. Waggie, B. Reardon and J. L. Ellsworth, *Osteoarthritis Cartilage*, 2005, **13**, 623–631.

This journal is © The Royal Society of Chemistry 2024

J. Mater. Chem. B, 2024, **12**, 10416–10433 | **10431**

27 T. Vinikoor, G. K. Dzidotor, T. T. Le, Y. Liu, H. M. Kan, S. Barui, M. T. Chorsi, E. J. Curry, E. Reinhardt, H. Wang, P. Singh, M. A. Merriman, E. D'Orio, J. Park, S. Xiao, J. H. Chapman, F. Lin, C. S. Truong, S. Prasadh, L. Chuba, S. Killoh, S. W. Lee, Q. Wu, R. M. Chidambaram, K. W. H. Lo, C. T. Laurencin and T. D. Nguyen, *Nat. Commun.*, 2023, **14**, 6257.

28 N. Peidavosi, M. Azami, N. Beheshtizadeh and A. Ramazani Saadatabadi, *Sci. Rep.*, 2022, **12**, 20828.

29 N. More, A. Srivastava and G. Kapusetti, *ACS Appl. Bio Mater.*, 2020, **3**, 6823–6835.

30 F. Barbosa, F. C. Ferreira and J. C. Silva, *Int. J. Mol. Sci.*, 2022, 23.

31 J. M. Patel, K. S. Saleh, J. A. Burdick and R. L. Mauck, *Acta Biomater.*, 2019, **93**, 222–238.

32 Z. H. Deng, Y. S. Li, X. Gao, G. H. Lei and J. Huard, *Osteoarthritis Cartilage*, 2018, **26**, 1153–1161.

33 M. A. Szychlinska, U. D'Amora, S. Ravalli, L. Ambrosio, M. Di Rosa and G. Musumeci, *Curr. Pharm. Biotechnol.*, 2019, **20**, 32–46.

34 L. A. Fortier, J. U. Barker, E. J. Strauss, T. M. McCarrel and B. J. Cole, *Clin. Orthop. Relat. Res.*, 2011, **469**, 2706–2715.

35 Y. Yang, X. Yin, H. Wang, W. Qiu, L. Li, F. Li, Y. Shan, Z. Zhao, Z. Li, J. Guo, J. Zhang and Y. Zhao, *Nano Energy*, 2023, **107**, 108145.

36 C. E. Kilmer, C. M. Battistoni, A. Cox, G. J. Breur, A. Panitch and J. C. Liu, *ACS Biomater. Sci. Eng.*, 2020, **6**, 3464–3476.

37 B. Xie, F. Yang, H. Chen, H. Zhang, H. Ma, T. Li, Z. Chen, J. Li, X. Li and J. Du, *Front. Mater.*, 2023, **10**, 1292098.

38 Y. Li, X. Dai, Y. Bai, Y. Liu, Y. Wang, O. Liu, F. Yan, Z. Tang, X. Zhang and X. Deng, *Int. J. Nanomed.*, 2017, **12**, 4007–4018.

39 K. Imamura, K. Tachi, T. Takayama, R. Shohara, H. Kasai, J. Dai and S. Yamano, *J. Biomater. Appl.*, 2018, **32**, 1382–1391.

40 K. L. Riedler, A. Shokrani, A. Markarian, L. M. Fisher and J. P. Pepper, *Laryngoscope*, 2017, **127**, E399–e407.

41 T. M. Campbell, K. Reilly, O. Laneuville, H. Uhthoff and G. Trudel, *Bone*, 2018, **106**, 42–51.

42 M. P. van den Borne, N. J. Raijmakers, J. Vanlauwe, J. Victor, S. N. de Jong, J. Bellemans and D. B. Saris, *Osteoarthritis Cartilage*, 2007, **15**, 1397–1402.

43 P. Mainil-Varlet, T. Aigner, M. Brittberg, P. Bullough, A. Hollander, E. Hunziker, R. Kandel, S. Nehrer, K. Pritzker, S. Roberts and E. Stauffer, *J. Bone Jt. Surg., Am.*, 2003, **85**(2), 45–57.

44 J. S. Wayne, C. L. McDowell, K. J. Shields and R. S. Tuan, *Tissue Eng.*, 2005, **11**, 953–963.

45 E. J. Curry, T. T. Le, R. Das, K. Ke, E. M. Santorella, D. Paul, M. T. Chorsi, K. T. M. Tran, J. Baroody, E. R. Borges, B. Ko, A. Golabchi, X. Xin, D. Rowe, L. Yue, J. Feng, M. D. Morales-Acosta, Q. Wu, I. P. Chen, X. T. Cui, J. Pachter and T. D. Nguyen, *Proc. Natl. Acad. Sci. U. S. A.*, 2020, **117**, 214–220.

46 Z. Li, P. Liu, T. Yang, Y. Sun, Q. You, J. Li, Z. Wang and B. Han, *J. Biomater. Appl.*, 2016, **30**, 1552–1565.

47 S. J. Hollister, *Nat. Mater.*, 2005, **4**, 518–524.

48 C. Shuai, G. Liu, Y. Yang, W. Yang, C. He, G. Wang, Z. Liu, F. Qi and S. Peng, *Colloids Surf., B*, 2020, **185**, 110587.

49 E. J. Curry, K. Ke, M. T. Chorsi, K. S. Wrobel, A. N. Miller, 3rd, A. Patel, I. Kim, J. Feng, L. Yue, Q. Wu, C. L. Kuo, K. W. Lo, C. T. Laurencin, H. Ilies, P. K. Purohit and T. D. Nguyen, *Proc. Natl. Acad. Sci. U. S. A.*, 2018, **115**, 909–914.

50 A. Gautieri, S. Vesentini, A. Redaelli and M. J. Buehler, *Nano Lett.*, 2011, **11**, 757–766.

51 A. Ode, G. N. Duda, S. Geissler, S. Pauly, J. E. Ode, C. Perka and P. Strube, *PLoS One*, 2014, **9**, e106462.

52 D. Khare, B. Basu and A. K. Dubey, *Biomaterials*, 2020, **258**, 120280.

53 S. M. Damaraju, Y. Shen, E. Elele, B. Khusid, A. Eshghinejad, J. Li, M. Jaffe and T. L. Arinzeh, *Biomaterials*, 2017, **149**, 51–62.

54 A. Wang, Z. Liu, M. Hu, C. Wang, X. Zhang, B. Shi, Y. Fan, Y. Cui, Z. Li and K. Ren, *Nano Energy*, 2018, **43**, 63–71.

55 L. Vannozzi, L. Ricotti, C. Filippeschi, S. Sartini, V. Coviello, V. Piazza, P. Pingue, C. La Motta, P. Dario and A. Menciassi, *Int. J. Nanomed.*, 2016, **11**, 69–91.

56 Y. Mori, T. Saito, S. H. Chang, H. Kobayashi, C. H. Ladel, H. Guehring, U.-I. Chung and H. Kawaguchi, *J. Biol. Chem.*, 2014, **289**, 10192–10200.

57 T. Shimoaka, T. Ogasawara, A. Yonamine, D. Chikazu, H. Kawano, K. Nakamura, N. Itoh and H. Kawaguchi, *J. Biol. Chem.*, 2002, **277**, 7493–7500.

58 Z. Zhou, J. Zheng, X. Meng and F. Wang, *Int. J. Mol. Sci.*, 2023, 24.

59 Y. Zhang, F. Yang, K. Liu, H. Shen, Y. Zhu, W. Zhang, W. Liu, S. Wang, Y. Cao and G. Zhou, *Biomaterials*, 2012, **33**, 2926–2935.

60 J. B. Jonnalagadda, I. V. Rivero and J. S. Dertien, *J. Biomater. Sci., Polym. Ed.*, 2015, **26**, 401–419.

61 C. Y. Ko, K. L. Ku, S. R. Yang, T. Y. Lin, S. Peng, Y. S. Peng, M. H. Cheng and I. M. Chu, *J. Tissue Eng. Regener. Med.*, 2016, **10**, E485–e496.

62 D. Schumann, R. Kujat, J. Zellner, M. K. Angele, M. Nerlich, E. Mayr and P. Angele, *Biorheology*, 2006, **43**, 431–443.

63 P. Xia, Y. Shi, X. Wang and X. Li, *Stem Cell Res. Ther.*, 2022, **13**, 214.

64 C. H. Lai, S. C. Chen, L. H. Chiu, C. B. Yang, Y. H. Tsai, C. S. Zuo, W. H. Chang and W. F. Lai, *Ultrasound Med. Biol.*, 2010, **36**, 1022–1033.

65 S. Müller, S. Lindemann and A. Gigout, *J. Orthop. Res.*, 2020, **38**, 653–662.

66 D. H. Sohn, L. M. Lottman, L. Y. Lum, S. G. Kim, R. A. Pedowitz, R. D. Coutts and R. L. Sah, *Clin. Orthop. Relat. Res.*, 2002, 254–262, DOI: **10.1097/00003086-200201000-00030**.

67 E. M. Darling and K. A. Athanasiou, *J. Orthop. Res.*, 2005, **23**, 425–432.

68 A. Gigout, H. Guehring, D. Froemel, A. Meurer, C. Ladel, D. Reker, A. C. Bay-Jensen, M. A. Karsdal and S. Lindemann, *Osteoarthritis Cartilage*, 2017, **25**, 1858–1867.

69 J. Jacob, N. More, C. Mounika, P. Gondaliya, K. Kalia and G. Kapusetti, *ACS Appl. Bio Mater.*, 2019, **2**, 4922–4931.

70 T. Shimoaka, T. Ogasawara, A. Yonamine, D. Chikazu, H. Kawano, K. Nakamura, N. Itoh and H. Kawaguchi, *J. Biol. Chem.*, 2002, **277**, 7493–7500.

10432 | *J. Mater. Chem. B*, 2024, **12**, 10416–10433

This journal is © The Royal Society of Chemistry 2024

71 S. D. McCullen, J. P. McQuilling, R. M. Grossfeld, J. L. Lubischer, L. I. Clarke and E. G. Loboa, *Tissue Eng., Part C*, 2010, **16**, 1377–1386.

72 N. J. Chang, M. Y. Shie, K. W. Lee, P. H. Chou, C. C. Lin and C. J. Chu, *Int. J. Mol. Sci.*, 2017, 18.

73 N. J. Chang, C. C. Lin, M. Y. Shie, M. L. Yeh, C. F. Li, P. I. Liang, K. W. Lee, P. H. Shen and C. J. Chu, *Acta Biomater.*, 2015, **28**, 128–137.

74 T. G. Morgan, A. D. Rowan, S. C. Dickinson, D. Jones, A. P. Hollander, D. Deehan and T. E. Cawston, *Ann. Rheum. Dis.*, 2006, **65**, 184–190.

75 D. M. Knapik, J. D. Harris, G. Pangrazzi, M. J. Griesser, R. A. Siston, S. Agarwal and D. C. Flanigan, *Arthroscopy*, 2013, **29**, 1722–1731.

76 N. J. Chang, C. C. Lin, C. F. Li, D. A. Wang, N. Issariyaku and M. L. Yeh, *Biomaterials*, 2012, **33**, 3153–3163.

77 M. Kapoor, J. Martel-Pelletier, D. Lajeunesse, J. P. Pelletier and H. Fahmi, *Nat. Rev. Rheumatol.*, 2011, **7**, 33–42.

78 D. Reker, C. F. Kjelgaard-Petersen, A. S. Siebuhr, M. Michaelis, A. Gigout, M. A. Karsdal, C. Ladel and A. C. Bay-Jensen, *J. Transl. Med.*, 2017, **15**, 250.

This journal is © The Royal Society of Chemistry 2024

J. Mater. Chem. B, 2024, **12**, 10416–10433 | **10433**